Supplementary Information for

https://doi.org/10.1021/acsbiomaterials.1c01259

Biodegradable Fiducial Markers for Bimodal Near-Infrared Fluorescence- and X-ray-Based Imaging

Żaneta Górecka[1,2], *Dariusz Grzelecki*[3,9], *Wiktor Paskal*[4], *Emilia Choińska*[1], *Joanna Gilewicz*[3], *Robert Wrzesień*[5], *Wojciech Macherzyński*[6], *Michał Tracz*[7], *Elżbieta Budzińska-Wrzesień*[8], *Maria Bedyńska*[3], *Michał Kopka*[4], *Agnieszka Jackowska-Tracz*[7], *Ewelina Świątek-Najwer*[10], *Paweł K. Włodarski*[4], *Janusz Jaworowski*[3], *Wojciech Święszkowski*[1*]

[1] Division of Materials Design, Faculty of Materials Science and Engineering, Warsaw University of Technology, Warsaw, Poland

[2] Centre for Advanced Materials and Technologies CEZAMAT, Warsaw University of Technology, Poleczki 19, 02-822 Warsaw, Poland

[3] Department of Applied Pharmacy, Medical University of Warsaw, Warsaw, Poland

[4] Centre for Preclinical Research, The Department of Methodology, Medical University of Warsaw, Poland

[5] Central Laboratory of Experimental Animal, Medical University of Warsaw, Warsaw, Poland

[6] Faculty of Microsystem Electronics and Photonics, Wroclaw University of Science and Technology, Wroclaw, Poland

[7] Institute of Veterinary Medicine, Department of Food Hygiene and Public Health Protection, Warsaw University of Life Sciences, Warsaw, Poland

[8] The Department of Histology and Embryology, Medical University of Warsaw, Warsaw, Poland

[9] Department of Orthopedics and Rheumoorthopedics, Professor Adam Gruca Teaching Hospital, Centre of Postgraduate Medical Education, Otwock, Poland

[10] Faculty of Mechanical Engineering, Wroclaw University of Science and Technology, Wroclaw, Poland

* wojciech.swieszkowski@pw.edu.pl

A1.Supplementary figures and tables

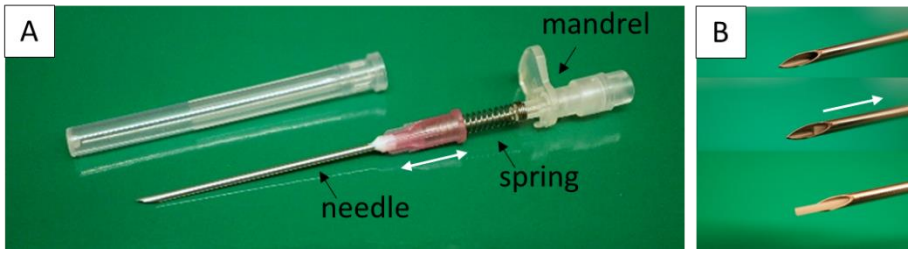

Figure S1 A) The device for Fiducia Marker (FM) implantation made of the mandrel of a peripheral venous catheter, metallic spring, and the needle G16; B) The operation mechanism of the device for FMs implantation - the marker is pushed out while the needle is pulled back.

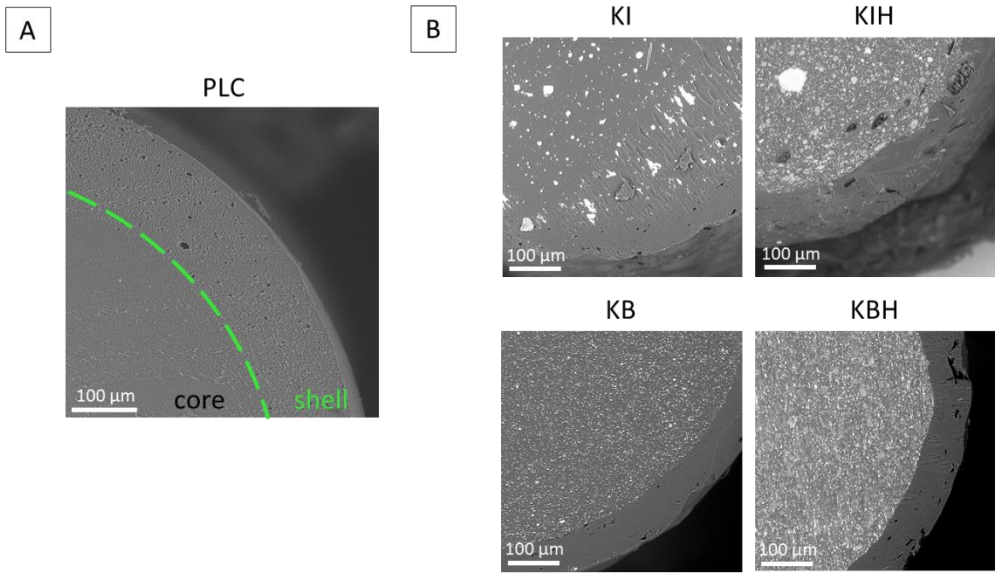

Figure S2 SEM images of cryo-ultramicrotome cross-sections of: A) as prepared PLC; B) KB, KBH, KI, and KIH markers before in vivo experiment (W0).

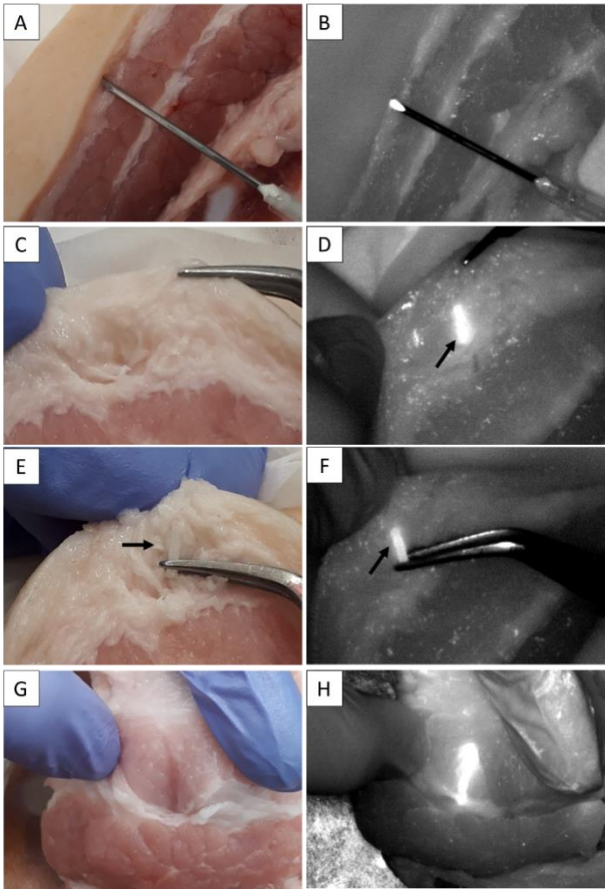

Figure S3 The naked-eye (**A, C, E, G**) and NIRF (**B, D, F, H**) images of P[LAcoCL] marker in a piece of pork belly (beacon) with skin, adipose, and muscle tissue: **A)** and **B)** implantation of FM into adipose tissue under the skin (thru skin imaging of the FM in comparison to peripheral venous catheter filled with 0.05 mg/ml ICG in iL solution can be found in **Figure 3E** of the Manuscript; **C)** and **D)** FM implanted in fatty tissue; **E)** and **F)** FM held in tweezers on a background of fatty tissue; **G)** and **H)** Marker implanted in muscle tissue. All NIRF images were taken in 5 – 30 gray values of the developed NIR system[1,2] to better contrast tissues.

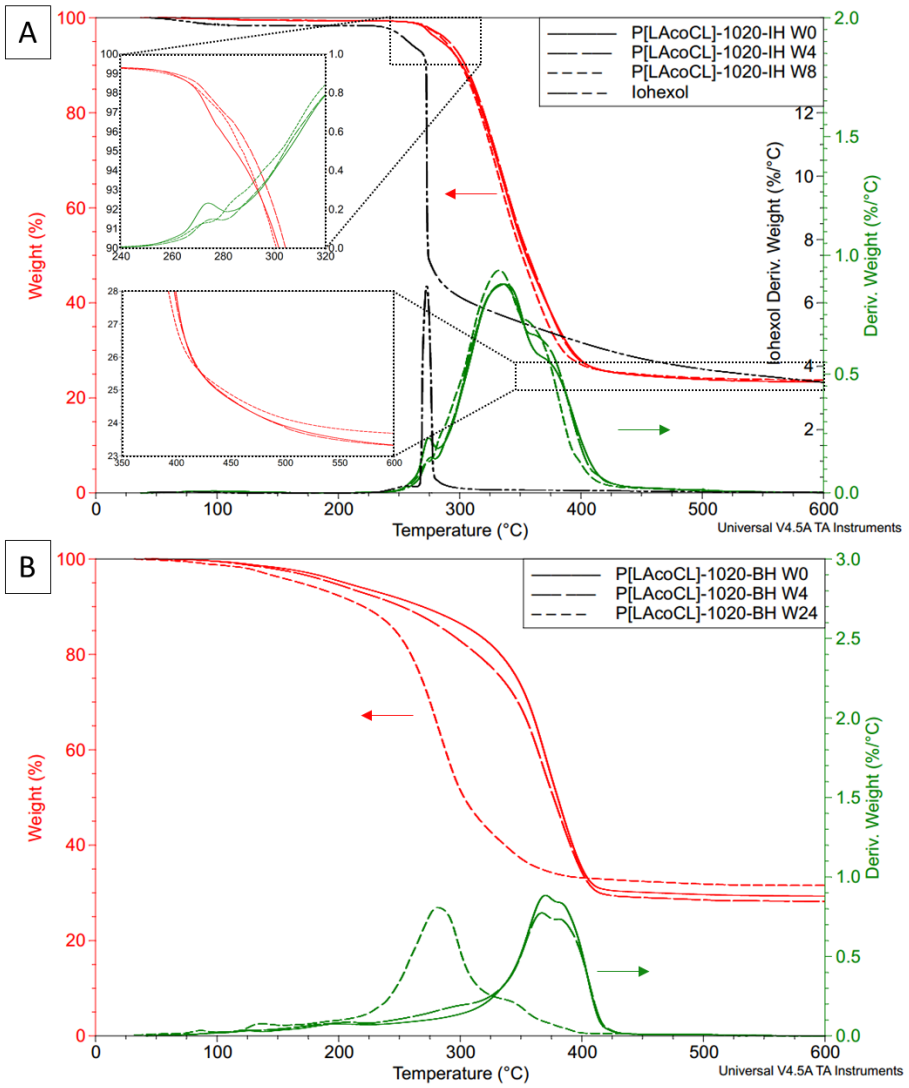

Figure S4 The TGA results of A) Iohexol powder and P[LAcoCL]-1020-IH at the beginning of degradation experiment; B) P[LAcoCL]-1020-BH samples at chosen time points of degradation experiment.

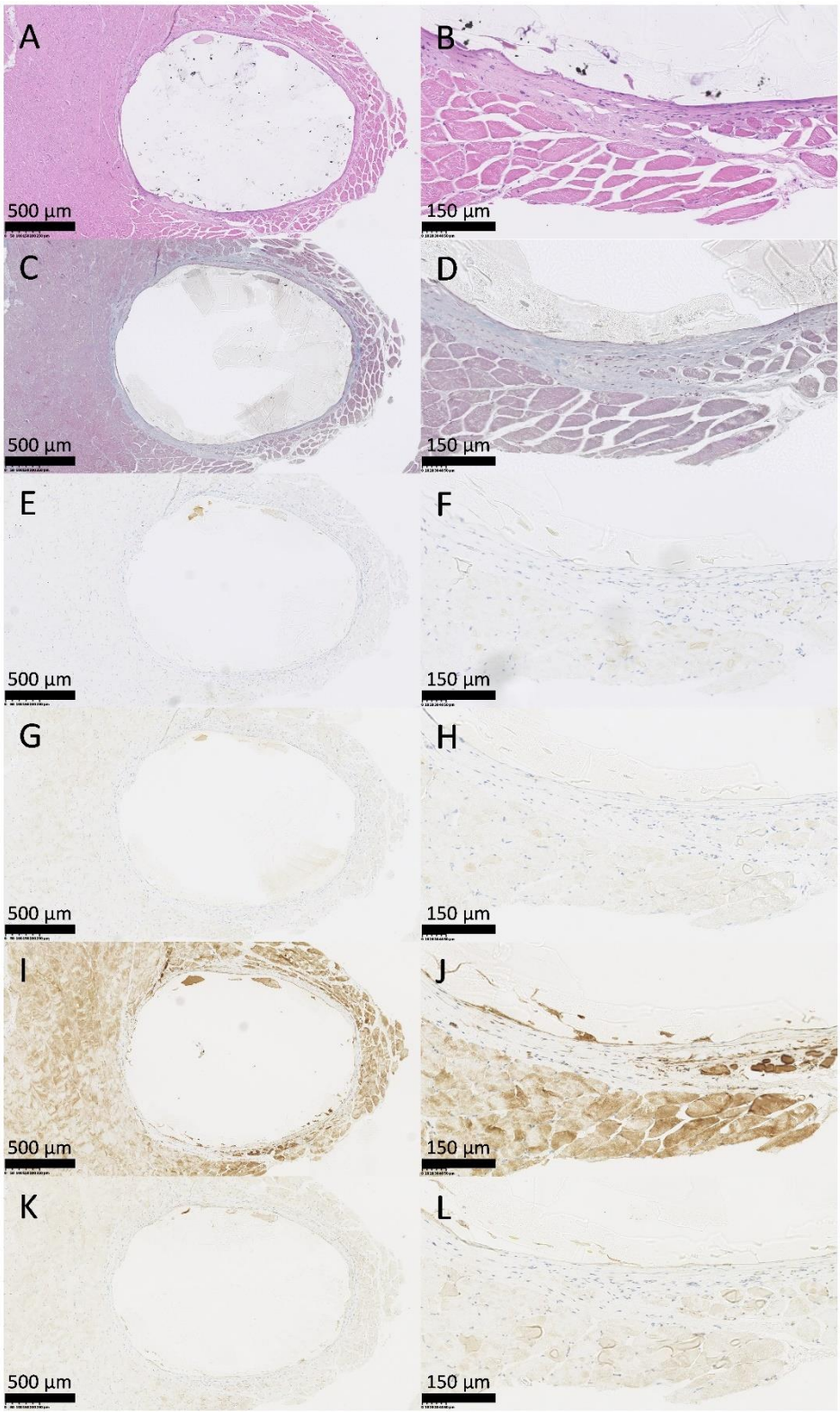

Figure S5 The representative sections of H&E (**A** and **B**), Masson's Trichrome (**C** and **D**), CD-31 (**E** and **F**), Il-1 (**G** and **H**), MMP-2 (**I** and **J**), and MMP-9 (**K** and **L**) stains with the place after the PLC marker implantation after the irradiation in 10x and 40x zoom, respectively.

Table S1 *Modified Jansen's scale. Adapted from* [3,4]

Reaction	Response	Grade
Reaction zone	Significant inflammatory cell infiltration: >30 inflammatory layers	**1**
	Medium inflammatory cell infiltration: 10-30 inflammatory layers	**2**
	Slight inflammatory cell infiltration: 5-9 inflammatory layers; incomplete layers of lymphocytes and macrophages	**3**
	Solitary cells of inflammatory infiltration: 0-4 inflammatory layer	**4**
Chronic inflammation	Five foreign body giant cells in the field of view (400) several layers of macrophages	**1**
	4-5 foreign body giant cells in the field of view (400) one layer of macrophages	**2**
	2-3 foreign body giant cells in the field of view (400) scattered foci of macrophages	**3**
	Fibroblasts contact implant surface without the presence of macrophages, 0-1 giant cell in the field of view (400)	**4**
Fibroblast capsule	Spindle-shaped fibroblasts and collagen fibers as a noncontinuous layer within the inflammatory layers, no signs of connective tissue organization	**1**
	Collagen fibers with many inflammatory cells	**2**
	Reactive tissue is fibrous but immature, showing fibroblasts and little collagen	**3**
	Apparent fibrous capsule (acellular), mature, non-dense, resembling connective tissue in non-injured regions	**4**
Muscle tissue structure	Fibrosis and fatty connective tissue	**1**
	Regenerating (recently necrotic)	**2**
	Necrotic myofibers	**3**
	Normal tissue (undamaged)	**4**

Table S2 Jansen's score results among the examined groups of rats depending on irradiation or not and type of implanted material. Evaluated according to the modified Jensen's scale (Table S1). The higher value, the more inert implant. Results were presented as a mean value (±SD). R - irradiated group; C- control group. p-value from Mann-Whitney U test analysis between R and C for all pairs of FMs. ^p-value from Kruskal-Wallis ANOVA analysis for all types of FMs within groups R and C for each parameter, separately.*Statistically significant differences in Mann-Whitney U test ($p<0.05$) were observed in chronic inflammation after the irradiation between the groups: PCL/KIH (p=0.034); KI/KIH (p=0.005); KI/KBH (p=0.02); KB/KIH (p=0.049); KB/KBH (p=0.023).

	Reaction zone			**Chronic inflammation**			**Fibroblast capsule**			**Muscle tissue structure**		
	R	**C**	***p***	**R**	**C**	***p***	**R**	**C**	***p***	**R**	**C**	***p***
PLC	3.78 (±0.44)	3.57 (±0.53)	0.52	2.88 (±0.6)	3.00 (±0.58)	0.79	2.44 (±0.72)	2.57 (±0.79)	0.96	2.11 (±0.78)	2.71 (±1.11)	0.29
KI	3.87 (±0.35)	3.14 (±0.69)	0.06	3.25 (±0.46)	3.43 (±0.98)	0.45	1.88 (±0.64)	2.29 (±0.48)	0.3	1.88 (±0.99)	2.43 (±0.53)	0.29
KB	3.75 (±0.46)	3.57 (±0.53)	0.60	3.25 (±0.46)	3.43 (±0.53)	0.6	2.25 (±0.46)	2.29 (±0.49)	0.95	2.38 (±0.74)	3.43 (±0.53)	**0.023**
KIH	3.44 (±0.52)	2.86 (±0.38)	0.09	2.11 (±0.6)	2.14 (±1.07)	0.91	2.11 (±0.33)	2.14 (±0.37)	0.96	2.33 (±0.86)	3.14 (±0.38)	0.09
KBH	3.44 (±0.52)	2.86 (±0.38)	0.09	2.11 (±0.93)	2.86 (±0.69)	0.17	2.44 (±0.53)	2.71 (±0.48)	0.4	2.22 (±0.44)	3.29 (±0.49)	**0.005**
^p	0.39	0.09	-	**0.004***	0.093	-	0.33	0.44	-	0.86	0.1	

A2.Detailed information about in vivo experiment

The study was performed on 48 mature male outbred rats from the WISTAR strain (8 weeks). Rats were housed in individually ventilated cages (IVC), fully protected by HEPA filters. Breeding parameters were established at 12h/12h day-night cycle. Environmental conditions were: the temperature at 20-24 ºC, the air humidity at 50% ±5%. Animals had ad libitum water access and were fed with balanced commercial pelleted diet dedicated for rat - LABOFEED B STANDARD (Wytwórnia Pasz "Morawski", Poland), composed of – proteins - 25%, fat - 8%, carbohydrates - 67% and fiber (crude) in valuated level for the mature animal. Animals were monitored daily for health status and were observed to identify any atypical behaviors. The animal study has been approved by the IInd Local Ethical Committee in Warsaw (animal experiment No. 360/2017 of 25.10.2017).

Before the surgical procedure, intraperitoneal anesthesia was performed with the injection of 10mg/100g ketamine (Bioketan, Vetoquinol Biowet, Poland) and 1mg/100g xylazine (Sedazin, Biowet Puławy, Poland) and one dose of enrofloxacin (Baytril 2,5%, Bayer, Germany). Subsequently, shaving and proper surgical field preparation with the aseptic principles were applied.

The implantation procedure did not require muscle or skin sewing. All rats received an intraperitoneal injection of natrium metamizole (Biovetalgin, Biowet Drwalew, Poland) immediately after the surgical procedure. No signs of local infection were noticed in the postoperative period. The day of implantation was described as day “0”.

Irradiation procedure

The irradiation procedure was performed on a Cobalt 60 gamma radiation source. The dose rate of 1,157 Gy/min was measured before the first cycle. The irradiation protocol was established according to the human cancer treatment protocols. Six cycles of total body irradiation (TBI) with a dose of 5 Gy were performed in the examined groups in weekly intervals (total dose 30 Gy). 5 Gy dose was delivered in approximately 4 min depending on the date of irradiation. The first dose was delivered 14 days after marker implantation and the last on the 49th day of the experiment. All rats were euthanized seven days after the last irradiation cycle on the 56th day of the experiment by a single injection of 0,5mg/kg pentobarbital (Morbital, Biowet Puławy, Poland).

Macroscopic observations in the day of euthanasia

At the end of *in vivo* experiment, there were no microscopical signs of infection, local inflammatory process, or post-radiation disease on the day of rats' euthanasia. The mean body weight of animals at the beginning of the experiment was 328g ±28g. Before the euthanasia, the average body weight of subjects in the non-irradiated group was 363g ±29g and in the irradiated group was 349g ±23g (p=0.13). One rat from KI/KB group died due to undiagnosed causes after the fourth radiation cycle and was excluded from the final analysis. The extended autopsy did not reveal the cause of death. Macroscopically, no signs of implant rejection were observed in all rats. However, in 3 cases, peri-implant hematoma in the irradiated group was noted (one for PLC and two for KIH markers).

A3.Details of histological and immunohistochemical staining

All implants were localized during the surgical section and harvested with at least a 10 mm diameter quadriceps muscle block. Samples were marked with red and blue dyes (CDI, Cancer Diagnostics INC., NC, USA) for proper orientation and individually inserted into the histological cassettes and preserved in formalin. Afterward, the samples were embedded in paraffin with an automatic tissue processor (ASP6026, Leica, USA). Each sample was manually oriented before the final paraffin embedding to produce sections perpendicular to the long axis of the implant. Then, paraffin blocks were cut on 3µm sections on a microtome and mounted on standard glass slides (Biosigma VBS656, Italy) or IHC-dedicated glass slides (IHC FLEX K8020, DAKO, Agilent, USA).

Sections underwent standard hematoxylin and eosin (H&E) staining with automatic tissue stainer (Leica). Implant-generated fibrous capsule thickness was measured manually in the optical microscope using a micrometric scale. The mean of three measurements in previously established points (12:00, 4:00, and 8:00 positions) for each sample was calculated. The local inflammatory response around the implants was measured according to the modified Jansen's scale (**Table S1**).[3,4]

Masson's Trichrome staining was used to visualize the collagen fibers. Deparaffinized sections were stained manually according to manufacturer guidelines (Sigma-Aldrich, HT15) and closed with a coverslip glass.

Immunohistochemical (IHC) staining, including five targets against specific cytokines, was done. Three cytokines, namely: *Interleukin-1 (*IL-1, ab106035, Abcam, diluted 1/1000), *Metalloproteinase 2 (*MMP-2, ab37150, Abcam, diluted 1/250), and *Metalloproteinase 9 (*MMP-9, AB19016, Merck, diluted 1/100) were chosen to evaluate the inflammatory

response. CD-31 cytokine (IR61061, Agilent -Dako, diluted 1/500) was adopted as an indicator of angiogenesis.[5–8] All antibodies were diluted with Dako Antibody Diluent (S3022, Dako). Deparaffinized sections underwent standard IHC staining protocol with Autostainer Link48 (DAKO) with EnVision FLEX+, High pH kit (K800221-2, Dako), which included: heat-induced antigen retrieval (High pH9,5 Buffer, K8004 Dako), endogenous peroxidase blocking with 3% hydrogen peroxide, primary antibody incubation, HRP/polymer incubation, and DAB addition. Antibodies dilution and staining specificity were verified on positive controls for each antibody. Stained slides were closed with glass coverslips. Stained sections were scanned on 20x magnification (NanoZoomer XR C9600-12, Hamamatsu). The whole slide images (WSI) of each slide were used for further analyses. IHC stained sections were also analyzed with a semi-automated protocol. WSI's were uploaded to QuPath v0.1.2.[9] WSI underwent "Simple tissue detection" followed by "Positive cell detection" modules. Combined modules enabled the detection of both stained and unstained cells and were finally expressed as the percentage of positive cells in the whole tissue section.

Masson's Trichrome stained WSI's were used to quantify fibrosis levels in muscle sections. WSI's were converted to .bmp images of resolution 6400x3616 px. Then, images were analyzed by a modified project designed by Sant'Anna et al. in CellProfiler.[10] Finally, the percentage of pixels containing collagen fibers in the section was calculated.

Statistical analysis in histological and immunohistochemical was performed with StatSoft STATISTICA 13.1 software (Tibco Software Inc., California, USA). The significance level was defined as $p<0.05$. Shapiro-Wilk test was used for determining the normality of data. Due to a small experimental group, the non-parametric Mann-Whitney U test was applied to determine the significance of the parameter differences of each marker

depending on the irradiation exposure. Kruskal-Wallis ANOVA test was used to evaluate potential differences across the different FMs in irradiated and non-irradiated groups.

A4. Detailed histological examination results

The experiment was designed to evaluate the difference between the tissue response to implanted FMs in a normal condition (non-irradiated) and under the irradiation procedure. The macroscopic observation of tissues surrounding the implants revealed no signs of infection, local inflammatory process, or post-radiation disease on the day of rats' euthanasia. Also, no signs of implant rejection were observed in all rats. However, in 3 cases, peri-implant hematoma in the irradiated group was noted (one for PLC and two for KIH markers). The detailed observations were described in supplementary data in section A3. Details of histological and immunohistological staining.

The macroscopic evaluation did not indicate an extensive inflammation process; however, the histological analysis of H&E slides revealed the infiltration of inflammatory cells in all cases. The infiltration of inflammatory cells (reaction zone) around all examined FMs in non-irradiated groups was more evident than in irradiated groups. However, the differences in the inflammatory response in specimens of the same implants, but irradiated and non-irradiated, and between the types of implants within the irradiated or non-irradiated groups were not significant. Similarly, the scores for the organization of the fibroblast capsule did not reveal significant differences. The representative images of the staining are presented in supplementary data **Figure S5**.

The results of the assessment of tissue specimens according to modified Jansen's scale were shown in **Table S2.** Briefly, in non-irradiated samples, the chronic inflammation comparison between all materials showed the most intensive response for the HAp-containing FMs. Nevertheless, the presence of HAp had a slightly better effect on the structure of the fibroblast capsule (KB vs. KBH) and muscle structure (KI vs. KIH). After the irradiation, a

statistically significant stronger chronic inflammation signal from HAP-containing FMs was also observed. However, the reaction zone was smaller than in the non-irradiated group and was similar to the other FMs. In general, no prominent differences between the same type of implant with or without irradiation were observed. Only for $BaSO_4$-containing FMs, significantly more evident muscle tissue damage around FMs was noted after the irradiation ($p=0.023$ and $p=0.005$, respectively). Moreover, in non-irradiated groups average thickness of the fibrous capsules around FMs was insignificantly larger than for irradiated groups; however, the differences were not significant (**Figure 7A** in Manuscript).

Semi-automatic, computer-assisted measurement of percentage occupancy by collagen fibers within the sections field (**Figure 7B** in Manuscript) revealed the increased fibrosis after the irradiation. No statistically significant differences were found in terms of the types of FMs from irradiated and non-irradiated groups. Likewise, a separate analysis of the pairs of implants, irradiated and non-irradiated, showed no differences.

The angiogenesis process was assessed indirectly through the surface CD-31 immunohistochemical visualization. The analysis of anti-CD-31 staining (**Figure 7C** in Manuscript) did not reveal the change in expression in irradiated tissues around marker with pristine P[LAcoCL] core when compared to the control unirradiated group ($p=0.86$). Among the rest of the FMs, significantly higher angio-suppression was observed in irradiated tissues; KI ($p=0.03$) and KIH ($p=0.002$), KB ($p=0.03$), and KBH ($p=0.008$). The subsequent analysis did not reveal the differences between the types of FMs in the non-irradiated groups. However, the FMs with HAp had lower mean values in irradiated groups. Moreover, tissues around the KIH marker after the irradiation showed the highest angio-suppression with statistically significant differences in comparison to KI ($p=0.024$), KB ($p=0.024$), and PLC ($p=0.024$) markers. The mean value of irradiated KBH was higher than KIH but noticeably lower than KB.

The immunohistochemical staining was also performed for Il-1, MMP-2, and MMP-9 cytokines (**Figure 7D, E, F** in Manuscript, respectively). After the irradiation, a higher intensity of inflammatory processes in muscle tissue was observed in all cases. However, separately, statistically significant differences were not found between the types of implants among irradiated and non-irradiated groups.

Higher expression of Il-1 around all FMs was observed after irradiation. However, the comparison of irradiated to non-irradiated groups showed statistically significant differences only in KBH (means 3.83±1.18% vs. 2.39±0.52%; p=0.045). The results for PLC with and without irradiation did not show significant differences (3.57±1.36% vs. 3.14±1.52%, p=0.67). The mean values of FMs with HAp were lower than the correspondent FMs without HAp, i.e., KIH<KI and KBH<KB.

For MMP-2 and MMP-9, no statistically significant differences were found. Nevertheless, it was revealed that after the irradiation, the expression of MMP-2 was higher than in the control groups. In the case of PLC, irradiation caused the most explicit increase in MMP-2 expression (38.28±6.75% for irradiated vs. 29.21±7.45% for control; p=0.1). Interestingly, the mean values of MMP-2 noted for KB and KBH were higher than for KI and KIH, respectively. Moreover, in HAp-containing groups (KIH and KBH), the response was lower than in PLC groups, whereas in groups without HAp were higher. For MMP-9, the lowest response was noted in the KIH group in both groups. Insignificantly higher values were observed for KBH groups, whereas, for FMs without HAp, the values were again slightly more elevated than for PLC.

References to SI:

(1) Majak, M.; Wojtków, M.; Żmudzińska, M.; Macherzyński, W.; Kulas, Z.; Popek, M.; Świątek-Najwer, E.; Żuk, M. A Preliminary Evaluation of a Basic Fluorescence Image Processing in Mentoreye System Using Artificially Prepared Phantoms. In *Advances in Intelligent Systems and Computing*; 2019; Vol. 762. https://doi.org/10.1007/978-3-319-91211-0_8.

(2) Swiatek-Najwer, E.; Majak, M.; Zuk, M.; Popek, M.; Kulas, Z.; Jaworowski, J.; Pietruski, P. The New Computer and Fluorescence-Guided System for Planning and Aiding Oncological Treatment. *International Journal of Computer Assisted Radiology and Surgery* **2017**, *12* (1 Supplement 1).

(3) Jansen, J. A.; Dhert, W. J. A.; van der Waerden, J. P. C. M.; von Recum, A. F. Semi-Quantitative and Qualitative Histologic Analysis Method for the Evaluation of Implant Biocompatibility. *Journal of Investigative Surgery* **1994**, *7* (2). https://doi.org/10.3109/08941939409015356.

(4) Mahdy, M. A. A. Skeletal Muscle Fibrosis: An Overview. *Cell and Tissue Research*. 2019. https://doi.org/10.1007/s00441-018-2955-2.

(5) Prudente, A.; Fávaro, W. J.; Filho, P. L.; Riccetto, C. L. Z. Host Inflammatory Response to Polypropylene Implants: Insights from a Quantitative Immunohistochemical and Birefringence Analysis in a Rat Subcutaneous Model. *International Braz J Urol* **2016**, *42* (3). https://doi.org/10.1590/S1677-5538.IBJU.2015.0289.

(6) Wang, J.; Liu, Y.; Zhang, L.; Ji, J.; Wang, B.; Jin, W.; Zhang, C.; Chu, H. Effects of Increased Matrix Metalloproteinase-9 Expression on Skeletal Muscle Fibrosis in Prolonged Alcoholic Myopathies of Rats. *Molecular Medicine Reports* **2012**, *5* (1). https://doi.org/10.3892/mmr.2011.592.

(7) Pierce, L. M.; Asarias, J. R.; Nguyen, P. T.; Mings, J. R.; Gehrich, A. P. Inflammatory Cytokine and Matrix Metalloproteinase Expression Induced by Collagen-Coated and Uncoated Polypropylene Meshes in a Rat Model. *American Journal of Obstetrics and Gynecology* **2011**, *205* (1). https://doi.org/10.1016/j.ajog.2011.02.045.

(8) Oviedo Socarrás, T.; Vasconcelos, A. C.; Campos, P. P.; Pereira, N. B.; Souza, J. P. C.; Andrade, S. P. Foreign Body Response to Subcutaneous Implants in Diabetic Rats. *PLoS ONE* **2014**, *9* (11). https://doi.org/10.1371/journal.pone.0110945.

(9) Bankhead, P.; Loughrey, M. B.; Fernández, J. A.; Dombrowski, Y.; McArt, D. G.; Dunne, P. D.; McQuaid, S.; Gray, R. T.; Murray, L. J.; Coleman, H. G.; James, J. A.; Salto-Tellez, M.; Hamilton, P. W. QuPath: Open Source Software for Digital Pathology Image Analysis. *Scientific Reports* **2017**, *7* (1). https://doi.org/10.1038/s41598-017-17204-5.

(10) Sant'Anna L. B.; Sant'Anna N.; Parolini O. Application of Computer Assisted Image Analysis for Identifying and Quantifying Liver Fibrosis in a Experimental Model. *Journal of Computational Interdisciplinary Sciences* **2011**, *2* (2). https://doi.org/10.6062/jcis.2011.02.02.0041.